*R*esearch in
*A*stronomy and
*A*strophysics

Dynamics of magnetic flux tubes and IR-variability of young stellar objects

Sergey Khaibrakhmanov[1,2], Alexander Dudorov[2] and Andrey Sobolev[1]

[1] Kourovka Astronomical Observatory, Ural Federal University, Ekaterinburg 620000, Russia; *khaibrakhmanov@csu.ru*

[2] Theoretical Physics Department, Chelyabinsk State University, Chelyabinsk 454001, Russia

Abstract We simulate the dynamics of slender magnetic flux tubes (MFTs) in the accretion disks of T Tauri stars. The dynamical equations of our model take into account aerodynamic and turbulent drag forces, and the radiative heat exchange between the MFT and ambient gas. The structure of the disk is calculated with the help of our MHD model of the accretion disks. We consider the MFTs formed at distances of $0.027 - 0.8$ au from the star with various initial radii and plasma betas β_0. The simulations show that MFTs with a weak magnetic field ($\beta_0 = 10$) rise slowly with speeds less than the speed of sound. MFTs with $\beta_0 = 1$ form an outflowing magnetized corona above the disk. Strongly magnetized MFTs ($\beta_0 = 0.1$) can cause outflows with velocities $20 - 50$ km s^{-1}. The tubes rise periodically over times from several days to several months according to our simulations. We propose that periodically rising MFTs can absorb stellar radiation and contribute to the IR-variability of young stellar objects.

Key words: accretion disks — instabilities — magnetohydrodynamics (MHD) — protoplanetary disks

1 INTRODUCTION

Various observations indicate that stars at the early stages of evolution (young stellar objects, YSOs (Adams et al. 1987)) have a magnetic field. Measurements of Zeeman splitting in their spectral lines show that classical T Tauri stars (Class II YSOs) have a surface magnetic field with strength $1 - 3$ kG (Johns-Krull 2007). Polarization maps of thermal emission from dust indicate that the accretion disks of these young stars have a large-scale magnetic field (Li et al. 2016, 2018). The angular resolution is still not enough to detect their magnetic field geometry in detail.

The theory of a fossil magnetic field predicts that the magnetic field of the accretion disks of young stars originates from the magnetic field of its parent molecular cloud (see for review Dudorov (1995); Dudorov & Khaibrakhmanov (2015)). The dynamo mechanism driven by turbulent cyclonic motions and differential rotation in conducting plasma can also lead to the generation of a magnetic field in the disk (see, for example, reviews Brandenburg & Subramanian (2005) and

Blackman (2012)). Some aspects of the dynamo action in accretion disks can be found in Brandenburg et al. (1995), Kitchatinov & Rüdiger (2010), Gressel & Pessah (2015) and Moss et al. (2016). In this work, we use the magnetohydrodynamics (MHD) model of accretion disks of young stars with a fossil magnetic field developed by Dudorov & Khaibrakhmanov (2014). Dudorov & Khaibrakhmanov (2014) have shown that the magnetic field geometry varies through the disk. The magnetic field is quasi-azimuthal, $B_\varphi \sim B_z$ (in cylindrical coordinates), in regions of thermal ionization, where the magnetic field is frozen in gas. Throughout most of the disk, Ohmic diffusion, magnetic ambipolar diffusion and the Hall effect operate (for example, see review Turner et al. (2014)). The magnetic field is quasi-poloidal, $(B_r, B_\varphi) \ll B_z$, inside regions with low ionization fraction ("dead" zones, Gammie (1996)), and quasi-azimuthal or quasi-radial, $B_r \sim B_z$, in the outer regions depending on the ionization parameters. The magnetic field has quasi-radial geometry near the borders of the "dead" zones (Khaibrakhmanov et al. 2017).

The intensity of the azimuthal magnetic field B_φ is amplified over a time scale on the order of the rotation period $P_{\rm orb}$. The intensity of B_r is amplified over an accretion time scale $t_{\rm acc}$. In the accretion disks $P_{\rm orb} \ll t_{\rm acc}$, therefore $B_r \ll B_\varphi$ in the inner region (see Dudorov & Khaibrakhmanov (2014)). The problem is what mechanism hinders significant growth of the azimuthal magnetic field in the region of thermal ionization. Dudorov & Khaibrakhmanov (2014) have assumed that magnetic buoyant force can be such a mechanism. Magnetic flux tubes (MFTs) form as a result of Parker instability of a gas layer with a strong horizontal magnetic field (see Parker (1979)). A number of numerical simulations confirmed the development of the Parker instability and formation of MFTs (Cattaneo & Hughes 1988; Matthews et al. 1995; Wissink et al. 2000; Fan 2001; Vasil & Brummell 2008). Once formed, the MFTs rise from the disk under the action of the buoyant force. This process leads to the escape of excess magnetic flux from regions where it is generated. Khaibrakhmanov et al. (2017) and Khaibrakhmanov & Dudorov (2017) incorporated magnetic buoyancy into the induction equation and showed that the buoyancy can be treated as an additional magnetic flux escape mechanism in the disks.

Usually, the MFT dynamics in accretion disks have been investigated in the frame of slender flux tube approximation (Sakimoto & Coroniti 1989; Torkelsson 1993; Chakrabarti & D'Silva 1994; Schramkowski 1996; Dudorov & Khaibrakhmanov 2016). The dynamics is determined by the buoyant force, drag forces, thermal structure of the disk, efficiency of heat exchange with ambient gas, and relation between the centrifugal and magnetic tension forces.

Dudorov & Khaibrakhmanov (2016) considered the dynamics of slender adiabatic MFTs in the accretion disks of young stars. In this paper, we extend their approach by including radiative heat exchange in the model equations. In the frame of the slender flux tube approximation, we investigate MFT dynamics in the accretion disks of T Tauri stars. The initial parameters take into account the disk structure determined using our MHD model of the accretion disks (Dudorov & Khaibrakhmanov 2014; Khaibrakhmanov et al. 2017). Different from other researchers, we take into account turbulent drag inside the disk. This paper is based on the talk presented at the "Stars and Interstellar Medium" section of the All-Russian Astronomical Conference VAK-2017 that was held on 2017 September 17C22 (see Samus & Li 2018 for review of the section).

The paper is organized as follows. In Section 2, we present our model of the MFT dynamics. The model of the accretion disk is briefly discussed in Section 3. Section 4 presents results of numerical simulations. Typical dynamics of the MFT is considered in Section 4.1. Dependence on the model parameters is investigated in Section 4.2. We make analytical estimates of the terminal MFT velocities in Section 4.3. We search for the observational appearance of MFT dynamics in Section 4.4. Section 5 summarizes and discusses our findings.

2 MODEL OF MAGNETIC FLUX TUBE DYNAMICS

We investigate the MFT dynamics inside the accretion disks using cylindrical coordinates (r, φ, z). Axis z coincides with the disk rotation axis. The magnetic field inside the disk has components $\boldsymbol{B} = (B_r, B_\varphi, B_z)$. We assume that toroidal magnetic field $\boldsymbol{B}_{\rm t} = (0, B_\varphi, 0)$ splits into MFTs due to Parker instability (Parker 1979). The MFT has the form of a torus around the disk rotation axis with major radius $a_{\rm maj} = r$ and minor radius $a \ll a_{\rm maj}$. The MFT is azimuthally symmetric. Therefore, we can investigate motion of the small part of the torus, i.e. a cylinder of unit length. This cylindrical MFT has radius a, gas pressure $P_{\rm g}$, density ρ, temperature T and magnetic field strength $B_\varphi = B$. The accretion disk is characterized by pressure $P_{\rm e}$, density $\rho_{\rm e}$ and temperature $T_{\rm e}$.

We model the dynamics of the MFT following Dudorov & Kirillov (1986) and use the system of equations

$$\rho \frac{d\boldsymbol{v}}{dt} = (\rho - \rho_{\rm e})\,\boldsymbol{g} + \rho \boldsymbol{f}_d\,(\boldsymbol{v}, \rho, T, a, \rho_e)\,, \quad (1)$$

$$\frac{d\boldsymbol{r}}{dt} = \boldsymbol{v}, \quad (2)$$

$$M_{\rm l} = \rho \pi a^2, \quad (3)$$

$$\Phi = B \pi a^2, \quad (4)$$

$$dQ = dU + P_{\rm e}dV, \quad (5)$$

$$P_{\rm g} + \frac{B^2}{8\pi} = P_{\rm e}, \quad (6)$$

$$\frac{dP_{\rm e}}{dz} = -\rho_{\rm e}g_z, \quad (7)$$

$$P_{\rm g} = \frac{R_{\rm g}}{\mu}\rho T, \quad (8)$$

$$U = \frac{P_{\rm g}}{\rho(\gamma - 1)} + \frac{B^2}{8\pi\rho}. \quad (9)$$

Equation (1) is the equation of motion (where $\boldsymbol{f}_d$ is the drag force per unit mass), (2, 3, 4) are the definitions of velocity $\boldsymbol{v}$, mass M_l per unit length and magnetic flux Φ of the MFT respectively, (5) is the first law of thermodynamics (Q is the heat per unit mass, $V = 1/\rho$ is the specific volume), (6) is the balance between internal pressure ($P = P_g + \frac{B^2}{8\pi}$) and external pressure (P_e), (7) is the equation of hydrostatic equilibrium for the disk, (8) is the equation of state (R_g is the universal gas constant, $\mu = 2.3$ is the molecular weight), (9) is the energy per unit mass and γ is the adiabatic index.

The first term on the right-hand side of Equation (1)

$$\boldsymbol{F}_b = (\rho - \rho_e)\,\boldsymbol{g}\,, \tag{10}$$

is the buoyant force, which is the difference between gravitational force and the force arising from Archimedes' principle, and $\boldsymbol{g}$ is gravitational acceleration.

We study the one-dimensional problem of MFT motion in the z-direction, so $\boldsymbol{v} = (0, 0, v)$, $\boldsymbol{r} = (0, 0, z)$ and $\boldsymbol{g} = (0, 0, g_z)$. Equality (6) shows that the MFT is lighter than the ambient gas, i.e. $\rho < \rho_e$. Therefore, the buoyant force $\boldsymbol{F}_b = (0, 0, F_b)$ causes the MFT to move upward. Drag force $\rho\boldsymbol{f}_d = (0, 0, \rho f_d)$ counteracts the motion. Aerodynamic drag force (see Parker (1979))

$$f_d = -\frac{\rho_e v^2}{2}\frac{C_d}{\rho\pi a^2}, \tag{11}$$

where C_d is the drag coefficient ~ 1. Turbulent drag force (Pneuman & Raadu 1972)

$$f_d = -\frac{\pi\rho_e\left(\nu_t a v^3\right)^{1/2}}{\rho\pi a^2}, \tag{12}$$

where ν_t is the turbulent viscosity. The latter is estimated as (Shakura & Sunyaev 1973)

$$\nu_t = \alpha v_s H, \tag{13}$$

where α is a non-dimensional constant characterizing the efficiency of turbulence,

$$v_s = \sqrt{\frac{R_g T_e}{\mu}} \tag{14}$$

is the isothermal speed of sound and H is the scale height of the disk.

Turbulent drag force (Eq. (12)) is taken into account inside the disk. Aerodynamic drag force (Eq. (11)) is considered above the disk.

The disk is assumed to be in hydrostatic equilibrium in the z-direction. The vertical component of stellar gravity,

$$g_z = -z\frac{GM_\star}{r^3}\left(1 + \frac{z^2}{r^2}\right)^{-3/2}, \tag{15}$$

where $M_\star$ is the mass of the star.

The system of equations (1-9) can be reduced to

$$\frac{dv}{dt} = \left(1 - \frac{\rho_e}{\rho}\right)g_z + f_d, \tag{16}$$

$$\frac{dz}{dt} = v. \tag{17}$$

$$a = a_0\left(\frac{\rho}{\rho_0}\right)^{-1/2}, \tag{18}$$

$$B = B_0\frac{\rho}{\rho_0}, \tag{19}$$

$$\frac{d\rho}{dt} = \frac{h_c P_T + U_T \rho_e g_z v}{P_T\left(U_\rho - \dfrac{P_e}{\rho^2}\right) - U_T\left(P_\rho + C_m\rho\right)}, \tag{20}$$

$$\frac{dT}{dt} = \frac{\rho_e g_z v\left(U_\rho - \dfrac{P_e}{\rho^2}\right) + h_c\left(P_\rho + C_m\rho\right)}{U_T\left(P_\rho + C_m\rho\right) - P_T\left(U_\rho - \dfrac{P_e}{\rho^2}\right)}, \tag{21}$$

$$\rho_e = \rho_m e^{-\frac{z^2}{2H}}, \tag{22}$$

where a_0, ρ_0 and B_0 are the initial radius, density and magnetic field strength of the MFT respectively, the subscript $_T$ means derivative with respect to T (with constant ρ), the subscript $_\rho$ means derivative with respect to ρ (with constant T), h_c is the heating power per unit mass, $C_m = \dfrac{B_0^2}{4\pi\rho_0^2}$, $H = v_s/\Omega$ is the scale height of the disk, $v_s = \sqrt{R_g T_e/\mu}$ is the isothermal sound speed and

$$\Omega = \sqrt{\frac{GM_\star}{r^3}} \tag{23}$$

is the Keplerian angular velocity.

Equations (18) and (19) follow from mass and magnetic flux conservation (Eqs. (3) and (4)). Equations (20) and (21) are derived from (5, 6 and 7). Heating power per unit mass is defined as $h_c = dQ/dt$. In the diffusion approximation

$$h_c \simeq -\frac{8}{3\kappa_R\rho^2}\frac{\sigma_R T^4 - \sigma_R T_e^4}{a^2}, \tag{24}$$

where κ_R is the Rosseland mean opacity and σ_R is the Stefan-Boltzmann constant. We determine κ_R as the power-law function of gas density and temperature following Dudorov & Khaibrakhmanov (2014).

Formula (22) is the solution of hydrostatic equilibrium Equation (7) in the isothermal case, T_e =const. We determine the surface of the disk as the locus $z = 3H$. Above the surface, temperature is constant T_e and density declines with height according to Equation (22) to the point where ρ_e becomes equal to the density of the interstellar medium $\rho_{ism} = 3.8 \times 10^{-20}\,\mathrm{g\,cm^{-3}}$.

3 MODEL OF THE DISK

We investigate the dynamics of the MFT in the accretion disk of a T Tauri star. We use our MHD model of accretion disks (Dudorov & Khaibrakhmanov 2014) to calculate the structure and magnetic field of the disks. Let us describe briefly the features of the model (see for details Dudorov & Khaibrakhmanov (2014) and Khaibrakhmanov et al. (2017)).

The model is an MHD-generalization of the Shakura & Sunyaev (1973) model. We solve the MHD equations in the stationary thin-disk that uses a thin stationary disk. It is assumed that turbulence is the main mechanism of angular momentum transport. The turbulent viscosity is estimated according to (13). The model has two main parameters: α and accretion rate $\dot{M}$.

The temperature of the disk is calculated from the balance between viscous heating and radiative cooling. We use low-temperature opacities from Semenov et al. (2003). Heating by stellar radiation and cosmic rays in the outer parts of the disk is also taken into account.

The magnetic field components are calculated from the induction equation taking into account Ohmic diffusion, magnetic ambipolar diffusion, magnetic buoyancy and the Hall effect. Ionization fraction is determined from the equation of collisional ionization (see Spitzer (1978)) considering ionization by cosmic rays, X-rays and radioactive decay, radiative recombinations and the recombinations on dust grains. Additionally, the evaporation of dust grains and thermal ionization are included in the model.

Outer boundary of the disk, r_{out}, is determined as the contact boundary, where the disk pressure equals the pressure of the external medium.

In Figure 1 we plot the radial profiles of the midplane temperature, surface density, midplane ionization fraction, vertical magnetic field strength and midplane plasma beta for a disk with $\alpha = 0.01$ and $\dot{M} = 10^{-7}\,M_\odot\,\mathrm{yr^{-1}}$. Stellar mass $M = 1\,M_\odot$. In the simulation, we have cosmic ray ionization rate $\xi_0 = 10^{-17}\,\mathrm{s^{-1}}$ and attenuation length $R_{CR} = 100\,\mathrm{g\,cm^{-2}}$, stellar X-ray

luminosity $L_{XR} = 10^{30}\,\mathrm{erg\,s^{-1}}$ and mean dust grain size $a_d = 0.1\,\mu\mathrm{m}$.

Figure 1 shows that the surface density and temperature gradually decrease with distance from the star. The temperature is $\sim 5000\,\mathrm{K}$ near the inner edge of the disk and $15\,\mathrm{K}$ near its outer edge at $r_{out} = 220\,\mathrm{au}$. In our model, the radial dependences of all physical quantities are power-law functions of the distance. Indexes of the power laws depend only on the parameters of opacity. The indexes change throughout the disk as the opacity changes. That is why the dependences $T(r)$ and $\Sigma(r)$ appear as piecewise-linear functions on a logarithmic scale in Figure 1. Typical slope of the temperature profile $p_T = -0.9$ in range $1 - 100\,\mathrm{au}$, and the typical slope of the surface density profile is $p_\Sigma = -0.7$. The latter is consistent with observations indicating that $p_\Sigma \in [0.4, 1]$ (Andrews et al. 2009).

The radial profile of B_z is more complex. In the innermost part of the disk, $r < 0.8\,\mathrm{au}$, the ionization fraction is high, $x > 10^{-10}$ and the magnetic field is frozen in gas. The radial profile of B_z follows the surface density profile in this region, and $B_z \simeq 170\,\mathrm{G}$ at the inner edge of the disk $r_{in} = 0.027\,\mathrm{au}$. The "dead" zone is situated at $r > 0.8\,\mathrm{au}$, where the ionization fraction is very low. Magnetic ambipolar diffusion reduces the magnetic field strength by 1–2 orders of magnitude in this region, so that typical $B_z(3\,\mathrm{au}) = 0.1\,\mathrm{G}$. Near the outer edge of the disk, the magnetic field is frozen in gas and its intensity is $4 \times 10^{-3}\,\mathrm{G}$. The plasma beta is not constant in the disk. It is ~ 100 near the inner edge of the disk, $\sim 10^4 - 10^5$ inside the "dead" zone and ~ 10 near the outer edge of the disk.

4 RESULTS

In this section, we present the results of simulations of the MFT dynamics in the accretion disks. The system of dynamical Equations (16, 17, 20, 21) is solved with the help of the explicit fourth order Runge-Kutta method with automatic selection of the time step and relative accuracy $\varepsilon = 10^{-6}$. At each time step, the radius and magnetic field strength of the MFT are calculated with the help of relations (18–19).

We assume that the MFT forms inside the disk at height $z_0 = [0.5, 1, 1.5]H$, in thermal equilibrium with the surrounding gas, $T_0 = T_e$, and with velocity $u_0 = 0$. We specify the initial magnetic field strength of the MFT
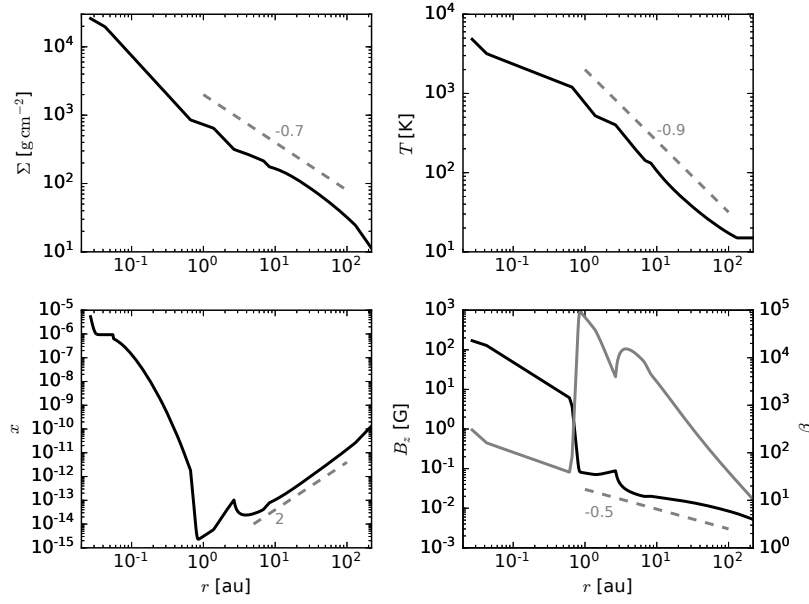
Fig. 1 The structure of the disk with $\alpha = 0.01$ and $\dot{M} = 10^{-7}\,M_\odot\,\mathrm{yr}^{-1}$ around a star with $M = 1\,M_\odot$. *Top left*: surface density, *top right*: midplane temperature, *bottom left*: midplane ionization fraction, *bottom right*: vertical magnetic field strength (left y-axis, *black line*) and plasma beta (right y-axis, *grey line*). *Grey dashed lines* with numbers depict typical slopes.

using plasma beta definition,

$$\beta_0 = \frac{8\pi P_{g0}}{B_0^2}, \tag{25}$$

where P_{g0} is the initial gas pressure inside the MFT. Initial density is determined from the condition of pressure equilibrium (6) at $t = 0$ in terms of β_0,

$$\rho_0 = \frac{P_e(z_0)}{\dfrac{R_g T_0}{\mu}\left(1 + \dfrac{1}{\beta_0}\right)}. \tag{26}$$

Adiabatic index of the molecular hydrogen gas $\gamma = 7/5$.

4.1 Fiducial Run

Let us first consider the typical picture of MFT dynamics. In the fiducial run, the dynamical Equations (16, 17, 20 and 21) are solved assuming that the MFT is at the distance $r = 0.027\,\mathrm{au}$ inside the disk. Parameters of the disk at this distance are as follows: temperature $T_e = 4830\,\mathrm{K}$, midplane density $\rho_m = 2 \times 10^{-6}\,\mathrm{g\,cm^{-3}}$, scale height $H = 6.2 \times 10^{-4}\,\mathrm{au}$ and magnetic field strength $B_z = 170\,\mathrm{G}$. Initial parameters of the MFT are: $a_0 = 0.1H$, $\beta_0 = 1$ and $z_0 = 0.5H$. In Figure 2, we plot the profiles of the velocity, drag and buoyant forces, densities ρ and ρ_e, and MFT radius.

The left panel of Figure 2 shows that initially MFT accelerates to the velocity $\simeq 0.7\ \mathrm{km\ s^{-1}}$ almost instantly, because the turbulent drag force is much less than

the buoyant force. After this acceleration, the drag force and buoyant force become nearly equal, $f_t \lesssim f_b$, and the MFT moves with increasing velocity. The acceleration decreases when the MFT rises to height $z \simeq 2.5 - 3H$. Above the disk, $z > 3H$, the acceleration tends to zero, as the buoyancy and aerodynamic drag forces become very small. The MFT moves by inertia with nearly constant velocity, $v \simeq 2\,\mathrm{km\,s^{-1}}$.

The MFT moves in a highly non-uniform medium. The right panel of Figure 2 shows that the MFT expands during its motion and its density decreases. External density also decreases with height. The difference in densities reduces from $50\,\%$ at the starting point to nearly zero at $z > 3H$, i.e. the degree of buoyancy decreases. The radius of the MFT becomes larger than the height of the disk at $z \simeq 4H$. Further motion of the MFT cannot be investigated in the frame of the slender tube approximation. We assume that the MFT dissipates at $z \simeq 4H$. The dissipation of the MFTs in the atmosphere of the disk leads to the formation of a non-stationary magnetized corona. The heating of the corona by dissipation of the magnetic field rising from the disk has also been found and discussed by Galeev et al. (1979) and Stella & Rosner (1984) in the context of accretion disks around black holes and by Miller & Stone (2000) in application to disks around classical T Tauri stars.

4.2 Dependence on Parameters

The dynamics of MFT depends on the initial position of the MFT inside the disk. In Figure 3, we present the dependence of the MFT velocity on the initial height and distance from the star. We consider three distances, $r = 0.027$ au (close to the inner boundary of the disk), $r = 0.15$ au ($T_e = 2025$ K, $\rho_m = 4.1 \times 10^{-8}$ g cm^{-3}, $H = 0.0053$ au, $B_z = 29.5$ G) and $r = 0.8$ au (outer zone of the thermal ionization region, where $T_e = 970$ K, $\rho_m = 8.3 \times 10^{-10}$ g cm^{-3}, $H = 0.045$ au, $B_z = 0.14$ G). The dynamics of the MFTs rising from $z_0 = 0.5H$, $z_0 = 1H$ and $z_0 = 1.5H$ are considered.

Figure 3 shows that the MFTs rapidly accelerate in the beginning, like in the fiducial run (see Sect. 4.1). After that, the MFTs rise with increasing velocity. Above the disk, $z > 3H$, the MFTs move with a constant velocity, that is ~ 1 km s^{-1} at $r = 0.8$ au and $2 - 2.5$ km s^{-1} at $r = 0.027$ au. Our simulations show that rise times to the surface of the disk are $0.5\,P_{\rm orb}$, $0.8\,P_{\rm orb}$ and $1.2\,P_{\rm orb}$ for the MFTs with $z_0 = 0.5H$, $z_0 = 1H$ and $z_0 = 2H$, respectively ($P_{\rm orb}$ is the rotation period).

4.3 Terminal Velocity of the MFT

As was shown in the previous section, after the initial acceleration, the MFT moves at a constant velocity, that is determined from the balance between the buoyant and drag forces. In the case of aerodynamic drag, we obtain the equality

$$\Delta\rho g_z = \frac{\rho_e v_b^2}{2} \frac{C_d}{\pi a^2}, \qquad (27)$$

where $\Delta\rho = \rho_e - \rho$. The difference in densities in thermal equilibrium is (see Eq. (6))

$$\Delta\rho = \frac{B^2}{8\pi v_s^2}. \qquad (28)$$

Substituting (28) into Equation (27), it is easy to derive the formula for calculating the terminal velocity (Parker 1979)

$$v_b = v_a \left(\frac{\pi}{C_d}\right)^{1/2} \left(\frac{a}{H}\right)^{1/2} \left(\frac{z_0}{H}\right)^{1/2}, \qquad (29)$$

where

$$v_a = \frac{B}{\sqrt{4\pi\rho}} \qquad (30)$$

is the Alfvén speed. Formula (29) shows that the terminal velocity of the MFT with $a \sim 1H$ at $z_0 \sim 1H$ approximately equals v_a. For convenience, we express the terminal velocity in terms of plasma beta and local speed of sound v_s

$$v_b = v_s \sqrt{\frac{2}{\beta}} \left(\frac{\pi}{C_d}\right)^{1/2} \left(\frac{a}{H}\right)^{1/2} \left(\frac{z_0}{H}\right)^{1/2}. \qquad (31)$$

Figure 4 shows dependences of the terminal velocity on the MFT radius for various plasma betas and initial heights z_0. Terminal velocities range from 2 to 50 km s^{-1} for radii in range $[0.1, 1]H$. The higher the initial height z_0 is, the more the terminal velocity of the MFT becomes. The MFTs with weak magnetic field ($\beta = 10$) move slowly with a velocity smaller than the speed of sound. The MFTs with strong magnetic field ($\beta = 0.1$) accelerate to velocities $\sim 40 - 50$ km s^{-1} characterizing molecular outflows. Generally speaking, a rising MFT can cause the outflows.

4.4 Buoyancy-driven Outflows

In Sections 4.1–4.3 we show that the MFT can form outflows from the disk. The buoyancy extracts magnetic flux from the disk over the time scale that the MFT rises to the surface of the disk. As we discussed in the Introduction, the toroidal magnetic field is permanently amplified in the region of thermal ionization. When the magnetic field reaches a state with $\beta \sim 1$, the MFTs form, rise from the disk and carry away the excess magnetic flux. Time scale of the magnetic field amplification can be estimated from the induction equation. In the approximations of the accretion disk model, the time scale of the azimuthal magnetic field amplification (see Dudorov & Khaibrakhmanov (2014)),

$$t_{\rm gen} = \frac{2}{3} \frac{|B_\varphi|}{|B_z|} \Omega^{-1} \left(\frac{z}{r}\right)^{-1}$$
$$\simeq 2.12 P_{\rm orb} \left(\frac{z/r}{0.05}\right)^{-1} \frac{|B_\varphi|}{|B_z|}. \qquad (32)$$

Formula (32) shows that $t_{\rm gen} \simeq 2P_{\rm orb}$ at height $z = 1H$.

Comparison of rise times discussed in Section 4.2 and estimate (32) shows that the rise time of MFTs is less than $t_{\rm gen}$. Therefore, the considered buoyancy-driven outflows are periodic. The period of the outflows will be on the order of the magnetic field amplification time scale, i.e. several rotation periods.

We propose that periodically rising MFTs can contribute to the variability of radiation emitted by YSOs. In the region $r = [0.5, 0.8]$ au, temperature $T \lesssim 1500$ K and MFTs contain dust grains. Such rising MFTs can absorb stellar radiation and re-emit it in infrared (IR). This process can be responsible for the IR-variability of YSOs.
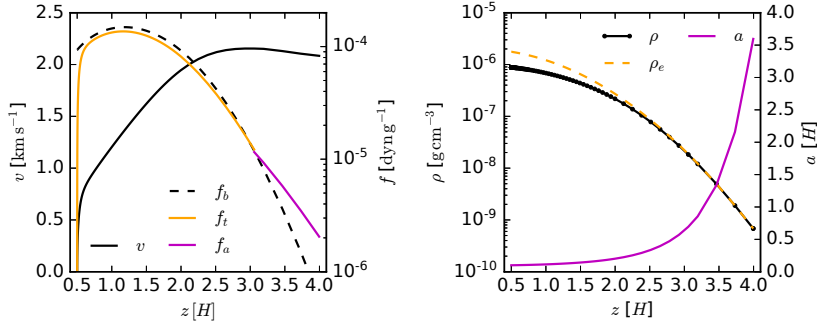
Fig. 2 *Left panel*: vertical profiles of the MFT velocity (left y-axis, *black line*) and forces per unit mass (right y-axis, *black dashed line*: buoyant force, *orange line*: turbulent drag force, *magenta line*: aerodynamic drag force). *Right panel*: vertical profiles of densities (left y-axis, *black line with dots*: MFT density, *orange dashed line*: disk density) and MFT radius (right y-axis, *magenta line*). Initial parameters: $a_0 = 0.1H$, $\beta_0 = 1$, $z_0 = 0.5H$.
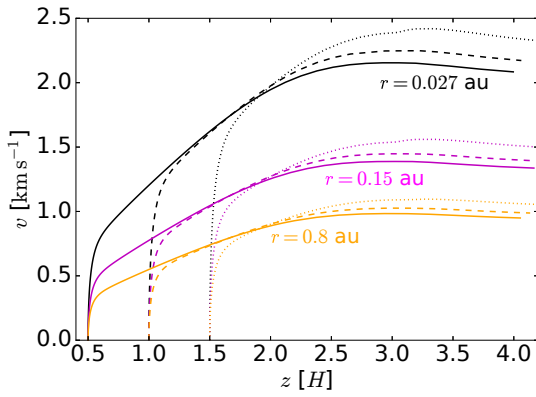

Fig. 3 Velocity profiles at distances $r = 0.027$ au (*black*), $r = 0.15$ au (*magenta*) and $r = 0.8$ au (*orange*) for different initial heights (*solid lines*: $z_0 = 0.5H$, *dashes*: $z_0 = 1H$, *dots*: $z_0 = 1.5H$).
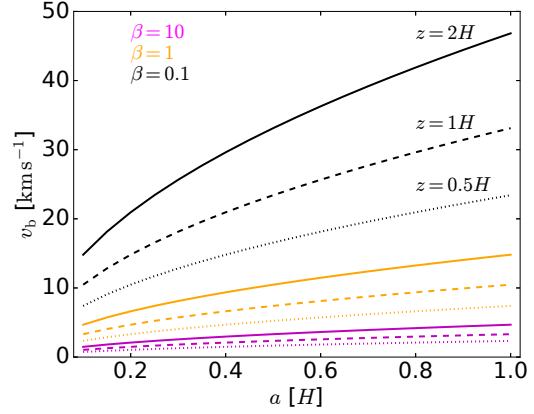
Fig. 4 Dependence of the terminal MFT velocity on radius of the MFT. *Black lines*: plasma $\beta = 0.1$, *orange lines*: $\beta = 1$, *magenta lines*: $\beta = 10$. *Solid lines*: $z_0 = 2H$, *dashed lines*: $z_0 = 1H$, *dotted lines*: $z_0 = 0.5H$.

The time scale of the variability would be on the order of the magnetic field amplification time scale, i.e. rotation periods. This time scale ranges from several days at $r = 0.027$ au to several months at $r = 0.8$ au.

5 CONCLUSIONS AND DISCUSSION

In this paper, we investigate the dynamics of MFTs in the accretion disks of young stars. In our previous paper, the adiabatic motion of MFTs was considered (Dudorov & Khaibrakhmanov 2016). Now we include the radiative heat exchange between the MFT and surrounding medium in the model. A disk in hydrostatic equilibrium is considered. The density, temperature and magnetic field strength of the disk are calculated with the help of our MHD model of accretion disks (Dudorov & Khaibrakhmanov 2014; Khaibrakhmanov et al. 2017).

We investigate the dynamics of the MFT with various initial radii a_0 and plasma beta β_0 formed at different distances from the star, $r = [0.027, 0.15, 0.8]$ au, and at different heights above the midplane of the disk, $z_0 = [0.5, 1, 2] H$. An accretion disk with turbulence parameter $\alpha = 0.01$ and accretion rate $\dot{M} = 10^{-7} \, M_\odot \, \text{yr}^{-1}$ around solar mass T Tauri star is considered.

The simulations show that MFTs rise from the disk to the atmosphere with velocities up to $\simeq 50 \, \text{km s}^{-1}$. The farther from the star the MFT formed, the less its terminal velocity. We divide the MFTs into two categories. Small MFTs (radius less than $\sim 0.1H$) cannot accelerate to speeds more than $10 \, \text{km s}^{-1}$. Large MFTs having radii more than $\sim 0.1H$ can reach velocities up to $50 \, \text{km s}^{-1}$.

The time needed for the MFT to rise to the surface of the disk is on the order of the rotation period. This time is less than the time scale of the toroidal magnetic

field amplification, t_{gen}. Therefore, the MFTs form inside the disk and float from it periodically over time scales $\sim t_{\mathrm{gen}}$, that range from several days to several months in the region of thermal ionization. The MFTs catastrophically expand above the disk.

The MFTs with weak magnetic field ($\beta = 10$) rise slowly with speeds less than the speed of sound. The MFTs with $\beta = 1$ form an outflowing magnetized corona. Strongly magnetized MFTs ($\beta = 0.1$) cause outflows with velocities $20 - 50 \, \mathrm{km \, s^{-1}}$. The outflow velocity is consistent with the velocity of molecular outflows from YSOs (see reviews Ray et al. (2007) and Frank et al. (2014)).

The MFTs that formed in the region of the disk with $T = [1000, 1500]\,\mathrm{K}$ contain dust particles. The rising MFTs will periodically absorb stellar radiation and re-emit it in IR. We propose that this process can contribute to the observational IR-variability found in many YSOs (see, for example, Flaherty et al. (2016)). Shadowing of the outer disk regions by periodically rising MFTs can also appear as IR-variability of the disk.

It should be noted that the specific mechanism of magnetic field generation is not important from the point of view of the dynamics of MFTs. Our conclusions can also be generalized for a dynamo-generated magnetic field in the disks.

In this work, an isothermal disk was considered. Several works investigated influence of radiation transfer on the vertical structure of protoplanetary disks (see, for example, Akimkin et al. (2013) and reference therein). We will consider the disk's thermal structure in detail in our next paper. We will investigate the influence of the magnetic field of the disk on MFT dynamics. It is also an interesting task to compare theoretical variability due to periodically rising MFTs with the IR-periodicity of YSOs.

References

Adams, F. C., Lada, C. J., & Shu, F. H. 1987, ApJ, 312, 788

Akimkin, V., Zhukovska, S., Wiebe, D., et al. 2013, ApJ, 766, 8

Andrews, S. M., Wilner, D. J., Hughes, A. M., Qi, C., & Dullemond, C. P. 2009, ApJ, 700, 1502

Blackman, E. G. 2012, Phys. Scr, 86, 058202

Brandenburg, A., Nordlund, A., Stein, R. F., & Torkelsson, U. 1995, ApJ, 446, 741

Brandenburg, A., & Subramanian, K. 2005, Phys. Rep., 417, 1

Cattaneo, F., & Hughes, D. W. 1988, Journal of Fluid Mechanics, 196, 323

Chakrabarti, S. K., & D'Silva, S. 1994, ApJ, 424, 138

Dudorov, A. E. 1995, Astronomy Reports, 39, 790

Dudorov, A. E., & Khaibrakhmanov, S. A. 2014, Ap&SS, 352, 103

Dudorov, A. E., & Khaibrakhmanov, S. A. 2015, Advances in Space Research, 55, 843

Dudorov, A. E., & Khaibrakhmanov, S. A. 2016, Astronomical and Astrophysical Transactions, 29, 429

Dudorov, A. E., & Kirillov, A. K. 1986, Byulletin Solnechnye Dannye Akademii Nauk SSSR, 1985, 85

Fan, Y. 2001, ApJ, 546, 509

Flaherty, K. M., DeMarchi, L., Muzerolle, J., et al. 2016, ApJ, 833, 104

Frank, A., Ray, T. P., Cabrit, S., et al. 2014, Protostars and Planets VI, 451

Galeev, A. A., Rosner, R., & Vaiana, G. S. 1979, ApJ, 229, 318

Gammie, C. F. 1996, ApJ, 457, 355

Gressel, O., & Pessah, M. E. 2015, ApJ, 810, 59

Johns-Krull, C. M. 2007, ApJ, 664, 975

Khaibrakhmanov, S. A., & Dudorov, A. E. 2017, Physics of Particles and Nuclei Letters, 14, 882

Khaibrakhmanov, S. A., Dudorov, A. E., Parfenov, S. Y., & Sobolev, A. M. 2017, MNRAS, 464, 586

Kitchatinov, L. L., & Rüdiger, G. 2010, A&A, 513, L1

Li, D., Pantin, E., Telesco, C. M., et al. 2016, ApJ, 832, 18

Li, D., Telesco, C. M., Zhang, H., et al. 2018, MNRAS, 473, 1427

Matthews, P. C., Hughes, D. W., & Proctor, M. R. E. 1995, ApJ, 448, 938

Miller, K. A., & Stone, J. M. 2000, ApJ, 534, 398

Moss, D., Sokoloff, D., & Suleimanov, V. 2016, A&A, 588, A18

Parker, E. N. 1979, Cosmical Magnetic Fields: Their Origin and Their Activity (Oxford: Oxford University Press)

Pneuman, G. W., & Raadu, M. A. 1972, ApJ, 172, 739

Ray, T., Dougados, C., Bacciotti, F., Eislöffel, J., & Chrysostomou, A. 2007, Protostars and Planets V, 231

Sakimoto, P. J., & Coroniti, F. V. 1989, ApJ, 342, 49

Samus, N. N., & Li, Y., RAA (Research in Astronomy and Astrophysics), 2018, 18, 88

Schramkowski, G. P. 1996, A&A, 308, 1013

Semenov, D., Henning, T., Helling, C., Ilgner, M., & Sedlmayr, E. 2003, A&A, 410, 611

Shakura, N. I., & Sunyaev, R. A. 1973, A&A, 24, 337

Spitzer, L. 1978, Physical Processes in the Interstellar Medium (New York: Wiley-Interscience)

Stella, L., & Rosner, R. 1984, ApJ, 277, 312

Torkelsson, U. 1993, A&A, 274, 675

Turner, N. J., Fromang, S., Gammie, C., et al. 2014, Protostars and Planets VI, 411

Vasil, G. M., & Brummell, N. H. 2008, ApJ, 686, 709

Wissink, J. G., Hughes, D. W., Matthews, P. C., & Proctor, M. R. E. 2000, MNRAS, 318, 501